

Modelling and performance analysis of a transparent multilayer solar cell

Maria Sultana Rupa, M. Tanseer Ali, Mohammad Abdul Mannan and Mehedi Hasan

Abstract— Transparent solar cells have emerged as a promising frontier in renewable energy research, offering the dual functionality of generating electricity while maintaining transparency. Five layers of InAs/InSb/AlGaAs/GaN/Si are incorporated into the proposed model structure which takes the properties of the source materials into consideration. Simulations of electromagnetic waves are used to evaluate optical and electrical properties. The cell is assumed to function at room temperature in the simulated settings. The I-V curve's fill factor (F.F.) of 0.6531 corresponds to a maximum conversion efficiency of 15.2655%, according to the data. Furthermore, at 530 nm, this combination and device configuration show a very good transparency of up to 60%.

Keywords — Transparent Solar Cell, COMSOL Multiphysics, Si, InAs, InSb, AlGaAs, GaN.

I. INTRODUCTION

Solar energy, in particular, is generating a boom in interest worldwide due to its widespread availability and environmental benefits over conventional fossil fuels [1]. Ongoing research encompasses different solar cell techniques, including silicon solar cells, dye-sensitized solar cells (DSC), organic polymer solar cells, hybrid solar cells, and CIGS solar cells [2]. Silicon was the first material to demonstrate high efficiency [3]. It is utilised in monocrystalline PV cells, which are at least 6% more efficient but also more costly than polycrystalline PV cells[4]. Polycrystalline cells have a slightly imperfect structure that hinders electron flow, though they are cheaper to produce. To address costly silicon, there's a growing demand for materials and methods that match efficiency while reducing expenses[5]. Researchers presented thin film PV cells (TFPV) as a low-cost option. Thin sheets cut semiconductor use in half, cutting costs by more than half. [6]

Maria Sultana Rupa
Department of EEE, American International University-Bangladesh, Dhaka, Bangladesh, email: mariasultana008@gmail.com

M. Tanseer Ali, Associate Professor, Department of EEE, Faculty of Engineering, American International University-Bangladesh, Dhaka, Bangladesh, Email: tanseer@aiub.edu

Mohammad Abdul Mannan, Professor and Associate Dean, Faculty of Engineering, American International University-Bangladesh, Dhaka, Bangladesh, Email: mdmannan@aiub.edu

Mehedi Hasan, Assistant Professor, Department of EEE, Faculty of Engineering, American International University-Bangladesh, Dhaka, Bangladesh, Email: mehedi@aiub.edu

Solar energy often needs much room to operate well and provide power to a building, either in the form of roofs or land; these solar panel space requirements are a significant barrier to practical use. Transparent solar cells (TSCs), which solve the problem by transforming any sheet of glass into a photovoltaic solar cell, were created due to this constraint. These cells efficiently utilise architectural space by generating electricity by collecting and using waste light energy from windows in buildings and automobiles.[7]. In terms of efficiency, single-junction solar cells have limited carrier

mobility and short diffusion lengths, which make it hard to widen the active charge layer for better spectrum absorption[8]. To address this, the 'tandem' concept is one of the simplest ways to boost power conversion efficiency[9].

Recently, significant efforts have been directed towards creating diverse tandem devices based on perovskite materials. These efforts involve optimising critical factors like the bandgap of absorber materials[10]. In the realm of efficiency, InGaP/(In)GaAs/Ge multijunction solar cells emerge as frontrunners, achieving remarkable levels of 29-32% efficiency under varying conditions[11]. Shifting the focus towards transparency, organic solar cells (DTDCTB: C70) take the lead with a notable light transmission of 66.4% at 530 nm, albeit with a trade-off in efficiency at 2.11%[12]. Hybrid thermal evaporation–spin coating technique striking a balance between these aspects, high-mobility hydrogenated indium oxide cells present an intriguing compromise, yielding a 14.2% efficiency and an impressive 72% average transmittance in the near-infrared range[13]. Notably, polyaniline-enhanced cells introduce a durability perspective, maintaining a 6.87% efficiency even after enduring 1500 bending cycles, underpinning their potential for robust applications.[14] Wrapping up the comparison, transparent a-Si: H cells, in tandem with thin metal electrodes, offer a versatile blend of 6.36% efficiency and 23.5% average transmittance (500–800 nm)[15].

In the current study, we describe the design and construction of a five-layer photonic structure that offers the best interference at each wavelength to achieve maximum efficiency while retaining extremely excellent transparency in the majority of the visible wavelengths.

The current work uses COMSOL Multiphysics to analyse a five-layer system comprising five materials used in those

layers. They are Si-Silicon, GaN- Gallium Nitride, AlGaAs- Aluminium Gallium Arsenide, InSb- Indium Antimonide and InAs- Indium Arsenide.

The FEMGEN software's model geometry ensures that elements are well meshed when mesh models are created based on variables like volume vs. circumradius, volume vs. dimension, rate of progression, and precondition number.

Using numerical methods, the fundamental idea of thermal and electrical impact at various temperatures has also been described. The range of the open circuit voltage, short circuit current and maximum power generated by the model is discovered and thoroughly explained. The numerical simulation is carried out using COMSOL Multiphysics Modeling Software.

II. THEORY AND METHODOLOGY

The electrical and optical components of the proposed model are examined in two steps utilising the 3D Finite Element Method (FEM) to determine the fundamental properties of each domain and their performance. The finite element method (FEM) is a computational approach to approximate boundary value problems resulting from partial differential equations. It is a mathematical approach often used to solve various engineering problems. Using the mesh construction technique, the entire domain of the structure is partitioned into discrete areas.

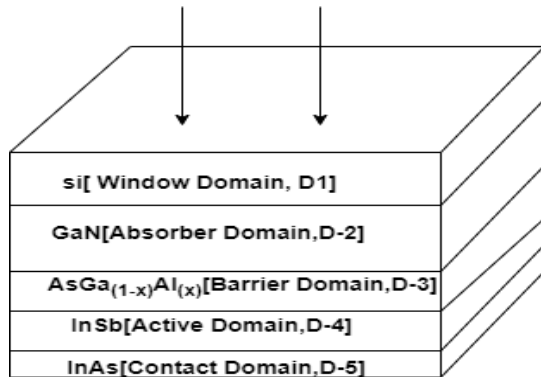


Fig 1: Domain Structure of transparent solar cell.

In Fig 1, Silicon (Si) and gallium Nitride Zinc Blende (GaN) work as the window & absorber materials having 12 eV 3.2 eV bandgap, respectively.

E_g (total band gap) (x) = (1.422 eV+) x (1.2475 eV) where $x < 0.45$ or $x = 0.3$ $Al_{0.3}Ga_{0.7}As$ works as the barrier, 0.17 eV & 0.354 eV bandgap of indium Antimonide (InSb) & Indium Arsenide (InAs) respectively as the active layer of bottom cell & ohmic metal contact which terminal voltage is 0V.

From the equation 1 to 6, these equations work for all domains at room temperature (300K) to find e proper result, its relative permittivity as ϵ_r , bandgap as $E_{g,0}$, electron affinity as χ_0 , effective density of states, valence and conduction band as N_v & N_c , electron & hole mobility as μ_n & μ_p . Those values are

taken from Table 1 for all materials. $n - p = p - n +$

$$N_d^+ - N_a^- \quad (1)$$

$$n = N_C \gamma e^{\frac{q(E_{f0} - E_C)}{kBTI}}; p = N_V \gamma e^{\frac{q(E_{fV} - E_C f_0)}{kBTI}} \quad (2)$$

$$J_n = n \mu_n \nabla E_C + q D_n \nabla n - q n D_n \nabla \ln(NC) + q n D_n, \text{th} \nabla \ln(T);$$

$$D_n = \mu_n kBTG \frac{n}{NC} \quad (3)$$

$$J_p = q p \mu_p \nabla E(V - q) D_p \nabla p + q p D_p \nabla \ln(NV) - q p D_p \text{th} \nabla \ln(T);$$

$$D_p = \mu_p kBTG \left(\frac{p}{NV} \right) \quad (4)$$

$$E_c = \pi r^2 = -(V + \chi_0), E_V = -(V + \chi_0 + E_g, 0) \quad (5)$$

$$E_{f0} = V e q, \text{adj} - V_0, \text{bias} \quad (6)$$

In the model, the continuity/ Heterojunction works in equation 7, which works with boundaries 2 to 5. No continuation exists, but a continuous quasi-fermi level works as its model.

$$E_{f_n,1} = E_{f_n,2} \quad E_{f_p,1} = E_{f_p,2} \quad D_1 = D_2 \quad (7)$$

Automatic initial values are working from 1 to 5 domains. Equations 8 and 9 which are work for electric potential and barrier potential as equation (7)

$$\Phi(x) = \frac{e N_d}{\epsilon_s} \left(x_n \cdot x - \frac{x^2}{2} \right) + \frac{e N_a}{2 \epsilon_s} x_p^2 \quad (0 \leq x \leq x_n) \quad (8)$$

$$V_b = |\phi(x = x_n)| = \frac{e}{2 \epsilon_s} (N_d x_n^2 + N_a x_p^2) \quad (9)$$

TABLE I

The wavelength of photons in different energy [8]

Colour	Wavelength (γ)	Frequency (F)	Photon energy
Violet	380-450nm	668-789THz	2.75-3.26eV
Blue	450-495nm	606-668THz	2.50-2.75eV
Green	495-570nm	526-606THz	2.17-2.50eV
Yellow	570-590nm	508-526THz	2.10-2.17eV
Orange	590-620nm	484-508THz	2.00-2.10eV
Red	620-750nm	400-484THz	1.65-2.00eV
Infrared	700-1050nm	430THz-300GHz	1.24meV-1.7eV

COMSOL Multiphysics 5.6a software was used to model the thin film solar cell. Five layers make up the entire device construction, as shown in Figure 1. The structure used for this investigation is based on a well-known scientific work cited as Ref. [16], which has achieved a remarkable global record efficiency of 12.6%.

III. MODEL DESIGN

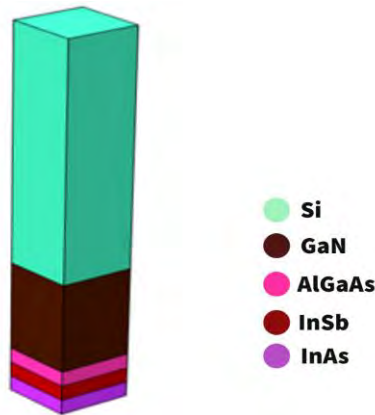


Fig 2: Model geometry

The photo absorption has been estimated, carrier photo-generation, carrier collection, and efficiency of this device taking into account the coupled optical and electrical simulation. To achieve this, we connected three multi-physics modules in COMSOL: the Semiconductor module, the Heat Transfer in Solid module, and the Electromagnetic Waves (Frequency domain) module. For the computation of the total photo-generation (G_{tot}), the Electromagnetic Waves module needed the optical constants, light intensity, and ideal conductor's characteristics. Within the semiconductor module, we included trap-assisted recombination and Shockley-Read-Hall: SRH recombination processes, requiring the materials and electrical characteristics.

By adjusting design parameters, we optimized our solar cell's performance and gained valuable insights into its behaviour under various conditions. With a height of 800 nm, the uppermost layer is modelled as Si. The subsequent layer, the 300 nm-deep GaN layer, is positioned behind this one. By simulating InSb and InAs layers at a thickness of 50 nm each, the interface between the GaN layer and the AlGaAs layer is created, and the AlGaAs layer thickness is maintained at 50 nm as we got better results in this thickness. InSb, which may be up to 50 nm thick, comes next, followed by InAs, the last layer, which is likewise 50 nm thick. Based on vector positioning considering air thickness the cell has a total size of 200 nm 200 nm 2950 nm. The referenced research and the material library in COMSOL Multiphysics are used for incorporating material characteristics.[16]

As found in Fig.2 material science-controlled network is determined for the calculation. The mesh configuration utilized in this study is based on a previous reference (Ref. [16]). The model's geometry makes use of an adjustable mesh, providing customization over variables such as the maximum and minimum element sizes, maximum element growth rate, and curvature factor.

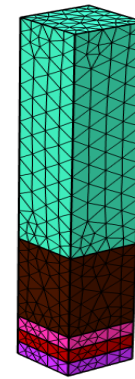


Fig 3: Mesh model

Careful consideration is given to achieve optimal resolution in narrow regions. A swept-type meshing approach is applied to all domains, with specific emphasis on the AlGaAs, InSb, and InAs layers due to their thin nature, necessitating finer meshing for accurate representation.

To bring a better quality of machine structure from previous machine quality, we used the most extreme equivalent and least component size of 18.75nm. There is bring a change of its machine size fine to most extreme level. For the complete geometry, the prior article defines a user-controlled mesh, as seen in 2.

The maximum and lowest element sizes for each domain individually mesh at 52.2 nm and 2.24 nm, respectively. With a curvature factor of 0.3, the maximum element growth rate is set at 1.35. As we found in Fig. 3 material science-controlled network is determined for the calculation. The most extreme component size is set to be 10nm, and the least component size is equivalent to 18.75 nm. The greatest component development rate is characterized to be 0.1, with the arch element as 0.8.

The chosen mesh configuration accurately represents the geometry while balancing computational efficiency. In the extent of this work, skewness quality measurement is picked in Fig. 3 Mesh model. The premise of picking this measurement over others is the grounds that this measurement is viewed as exceptionally dependable and is most famous in displaying procedures. The measure characterizes the lattice components as per their precise skewness. Elements deviating from the ideal lattice (concerning huge or little points) are punished.

Skewness near or equivalent to 1 is characteristic of an ideal cross-section component, while skewness near 0 addresses a declined part. Accordingly, in light of the skewness quality measurement, the characterized network is reasonable for further examination.[17].

TABLE II
Parameter of optical-electrical and thermal properties from COMSOL Multiphysics 5.6a

Parameter	Si	GaN	AlGaAs	InSb	InAs
Relative permittivity ϵ_r	11.7	9.7	12.9	16.8	15.15
Conduction band/valence band (Nc/Nv)	$1^{3/2} \times 2.8e^{19}/1^{3/2} \times 1.04e^{19}$	$1^{3/2} \times 2.3e^{14}/1^{3/2} \times 8e^{15}$	-	$1^{3/2} \times 8e^{12}/1^{3/2} \times 1.4e^{15}$	$1^{3/2} \times 1.68e^{13}/1^{3/2} \times 1.27e^{15}$
Electron mobility/hole mobility (μ_n/μ_p)	1450/500	1000/350	-	$7.7e^4/850$	$4e^4/5e^2$
Electron affinity (χ)	4.05	4.1	-	4.59	4.9
Bandgap (E_g)	1.12	3.2	-	0.17	0.354
Electron lifetime/Hole lifetime (τ_n/τ_p)	10us/10us	0.1ns/0.1ns	32ns/32ns	$5 \times 10^{-8}/5 \times 10^{-8}$	$3 \times 10^{-8}/3 \times 10^{-8}$
Acceptor/ Donor (N_A/N_D)	$1e^{19}/1e^{16}$	$1e^{19}/1e^{16}$	$4.3e^{19}/1e^{16}$	$1e^{19}/1e^{16}$	$1e^{19}/1e^{16}$
Thermal conductivity, (K)	131	130	$55-212 \times \text{def.x} + 248 \times \text{def.x}^2$	18	27
Space-charge thickness (ρ)	2329	6070	$5320-1560 \times \text{def.x}$	5770	5680

TABLE III

The value of the refractive index and extinction coefficient of all domain materials. [18-22]

Material	Refractive index(n)	Extinction coefficient(k)	Thickness (nm)
Si	3.88163	0.01896923	800
GaN	2.37966	0	300
$Al_xGa_{(1-x)}As$	3.81027	0.03467778	50
InSb	4.25505	1.801727	50
InAs	3.96317	0.6065408	50

TABLE IV

x -composition of $Al_xGa_{(1-x)}As$; $E_g(x)$ eV as Band gap, λ_g [nm] as wavelength gap. [23]

x	$E_g(x)$	λ_g
0	1.422	872
0.05	1.48	838
0.10	1.55	800
0.15	1.61	770
0.20	1.67	743
0.25	1.73	717
0.30	1.80	689
0.35	1.86	667
0.40	1.92	646
0.45	1.98	626
0.50	2.00	620
0.55	2.02	614
0.60	2.05	605
0.65	2.07	599
0.70	2.11	588
0.75	2.16	574

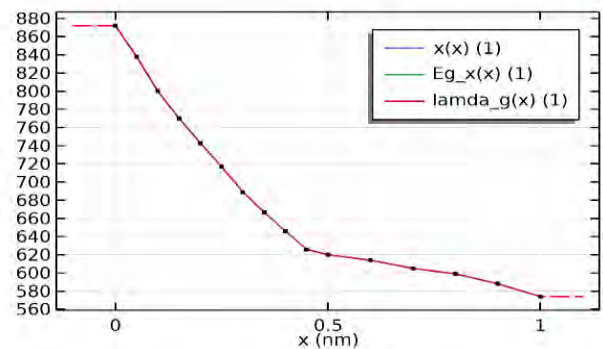


Fig 4 : Energy band gap of $Al_{(0.3)}Ga_{(0.7)}As$ alloys where $x=0.3$ based on table 3

In Fig.4, x -composite vs bandgap shows that the bandgap of AlGaAs alloys increases as the fraction of aluminum increases. This means that AlGaAs alloys with a higher fraction of aluminum will absorb light with shorter wavelengths. For example, $Al_{(0.3)}Ga_{(0.7)}As$ alloys have a bandgap of 1.9 eV, meaning they will absorb light with wavelengths of 650 nm or less.

IV. SIMULATION, DISCUSSION, RESULTS

At fig 5, an energy level diagram has been shown at room temperature where the quasi hole and valence band overlap and the valence band increases up to 0 points and slightly overlaps with the quasi electron.

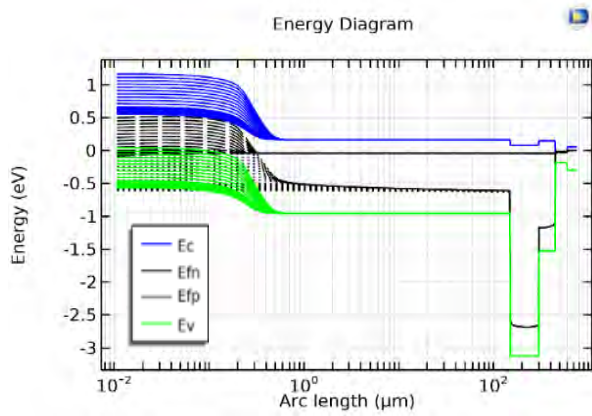


Fig 5: Energy level diagram

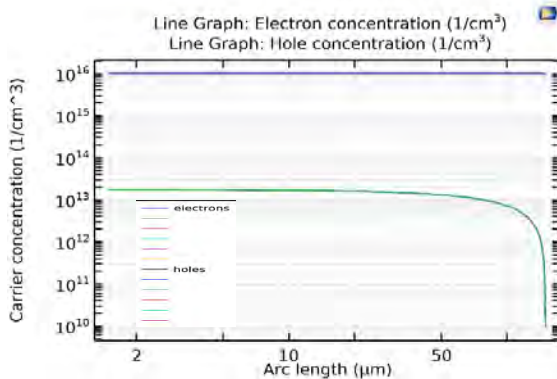


Fig 6: Carrier concentration of semiconductor

The change of concentration of junction of $Al_{(x)}Ga_{(1-x)}As$ is shown in this figure 6, $1e^{16}[cm^3]$ donor is taken as concentration for intersection and $4.3e^{19}[cm^3]$ as acceptor concentration also working for the junction. Free transporters are anticipated to absorb radiation with energy below the retention edge. The free opening retention coefficient is generally autonomous of frequency, while free electron ingestion shifts as λ^2 . In the free-transporter retention locale, the lessening coefficient increases with temperature and is a component of material deeping.

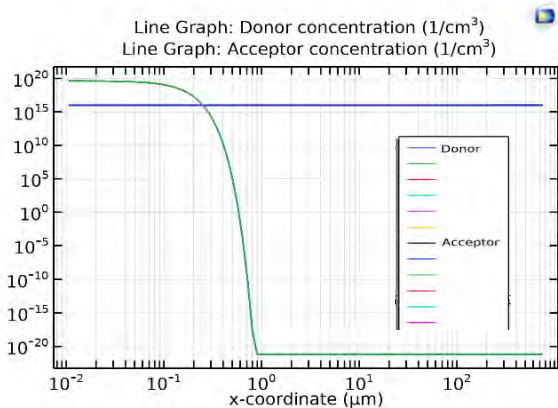


Fig 7: Doping level of semiconductor

Fig.7 shows donor concentration is approximately the same at $10^{15}[1/cm^3]$ point, but acceptor concentration shows near $10^{20}[1/cm^3]$. N_D is $1e^{16}[cm^3]$, and N_A is $4.3e^{19}[cm^3]$. Both are the centralization of the giver and acceptor molecules individually. In the space-charge area, the convergences of greater part charge transporters decline quickly. This reality permits us to utilize the supposition that the space charge.

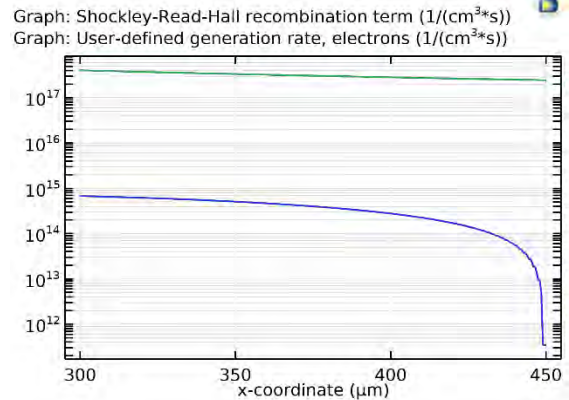


Fig 8 : Shockley-Read-hall recombination

In this fig. 8 above, SRH shows the recombination rate changes as the generation rate also changes its own position. The generation rate is staying approximately near to $10^{15}(1/cm^3 \times s)$ position.

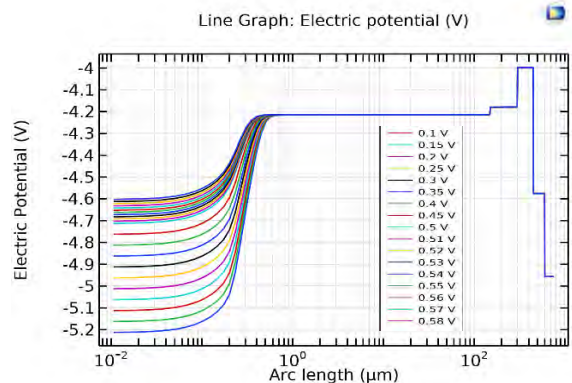


Fig 9: Electric potential of model semiconductor

In this Fig.9, Electric potential achieve quadratic dependence distance of the energy band diagram, which goes through inside the junction where the magnitude of this electric potential of $x=x_n$ is equal to barrier potential. Electric potential is the p region starting from -4.6V and saturates when it crosses the p region and enters the n region. After a certain time, it fell down to -5V. The electric potential increase or is highest in the p-n junction. Here, the x-axis plot or arc length from $10^{0.7}$ to $10^{2.2}$ is the highest p-n junction place where voltage works 4.6 to 4.9V. But when the potential goes to $10^{2.3}$ regions, and the voltage is works at -5, there is no p-n junction, and that's why the electric potential decrease until it goes to zero at the edge of the plot or cell.

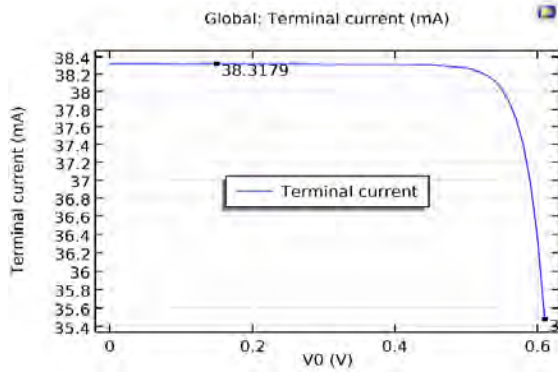


Fig 10: *I-V plot of model semiconductor*

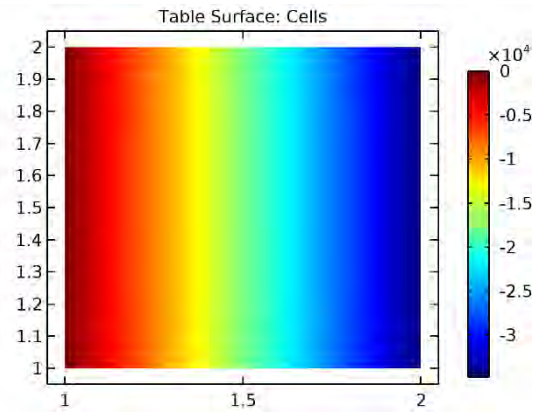


Fig 13: *Temperature-Current plot(2D)*

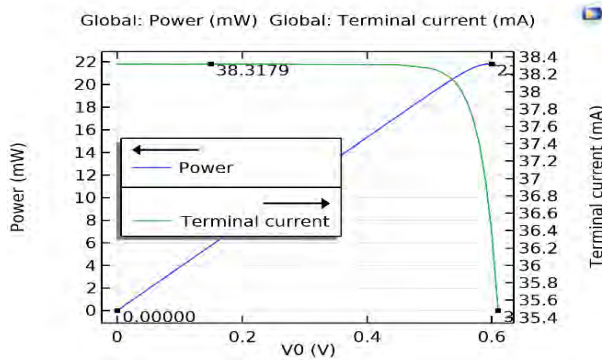


Fig 11: *P-V, I-V plot in model semiconductor*

TABLE V

The temperature value of sunlight heating vs creating terminal current in solar cell for temperature 310 K to 400K.

Temperature (K)	Terminal current (mA)	Temperature (K)	Terminal current (mA)
360.00	38.540		
310.00	38.545		
360.00	38.540		
330.00	38.545	350.00	38.541
360.00	38.541	310.00	38.545
330.00	38.545	390.00	38.542
370.00	38.540	340.00	38.545
		390.00	38.541
		310.00	38.545
		350.00	38.541

From Fig. 10 and 11, We obtained Fill factor = 0.6531 (I-V and P-V curves), enabling us to read off important working characteristics like the open circuit voltage 0.61 V, the short circuit current 38.3179 mA, and the maximum power 21.81 mW. From Fig. 10(P-V plot), we got efficiency=0.152655 or 15.2655% & its maximum power as $P_{max}=0.0153W$. In P-V, full control is approximately 21.81 mW, which comes from the I-V curve.

The model needs the irradiance of the incident sunlight, reflection off the module's top surface, and the module's electrical operational point to be heated. The P.V. module's ability to absorb sunlight in areas not covered by solar cells and the solar cells' ability to absorb low-energy (infrared) light. For temperature 300K, there is a temperature difference at a certain point. For the 1D plot, the current is 38.3129mA at 198K point and 38.3183mA at 239K. But for 2D plots, the temperature is highest below cells where light is absorbed highest level. Its shape also shows a square.

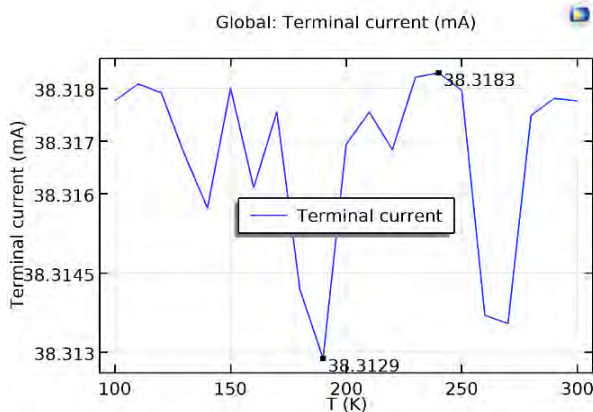


Fig 12: *Temperature- Current plot (1D)*

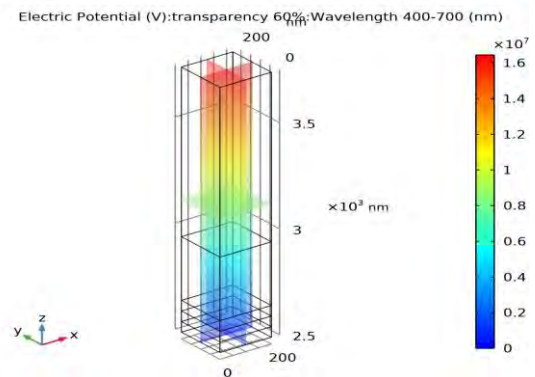


Fig 14: *Transparency vs wavelength (3D)*

In Figure 14, the transparency feature was applicable to the entire module. At a temperature of 300[K], all materials absorbed photon energy from the Sun's light. The top part of the module utilizes Si material to collect photon energy, and some of that energy was also allowed to pass through the module as a result of Si's transparency. The GaN material absorbs photon energy and contributes to the transparency of the module. AlGaAs acted as a p-n junction, allowed photon energy to pass through the entire module and contributing to its transparency. The active layer of InSb and the bottom layer of InAs material collected photon energy through their wavelengths and distributed it throughout the module. Overall, the module had a transparency of approximately 60[%], which was given the appearance of a transparent solar module.

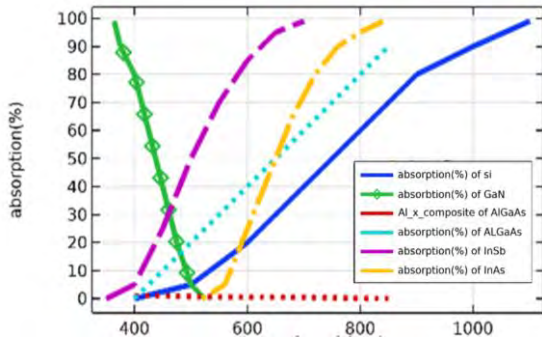


Fig 15: Absorption vs Wavelength

In this Fig 15, the slight bandgap Si, InSb, and InAs afford the extreme outcomes during the procedure of energy light absorption. InAs resources with extremely low bandgap's exhibition the extreme stages of absorption. Number of photon absorbed= Total absorption/Energy of one photon
 For Si, GaN, AlGaAs, InSb, InAs, the energy of one photon 1.12[eV], 3.79[eV], 2.48[eV], 2.84[eV], 2.37[eV]; total absorption 394% or 3.94, 394% or 3.94, 450% or 4.50, 429% or 4.29, 504% or 5.04; the number of photon absorbed 3.517 [eV], 1.039 [eV], 1.81 [eV], 1.51 [eV], 2.13[eV] for wavelength 1100 [nm], 525 [nm], 800 [nm], 700 [nm], 840 [nm].

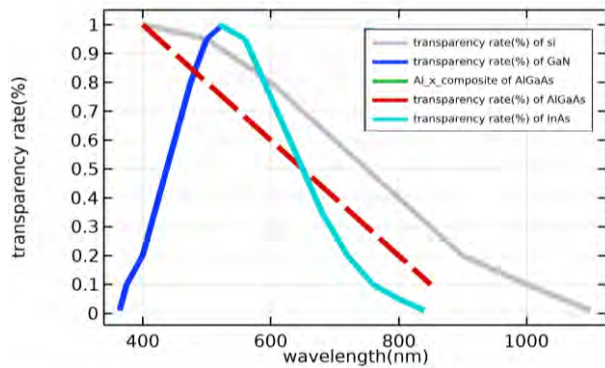


Fig 16(a): Transparency rate vs Wavelength with Si

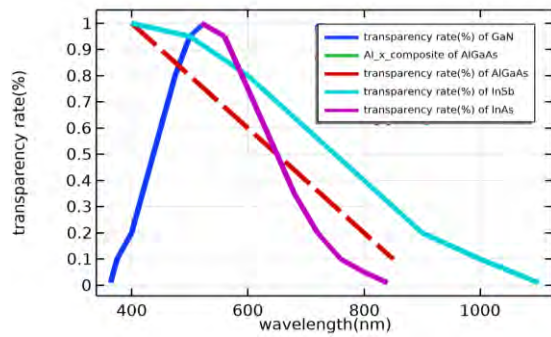


Fig 16(b): Transparency rate vs Wavelength without Si

For fig 16 (a) and 16 (b) , the high transparency rate of Si, InSb, InAs layers where light intensity is extremely high in top and bottom level whether photocurrent is also enlarged. In fig 16(a) and fig 16(b) where high absorption working for Si and InSb materials and there transparency rate quite similar that's why when one is active another one is invisible. With the help of the highest wavelength, the absorbance level is too high for Si material, which is acting as the electron transport layer.

For GaN material, photon light absorbing for wavelengths 364 & 375 [nm] is not working for photon light absorbing cause of ultraviolet light. The visible range can be observed in the cells with the Si, GaN, AlGaAs, InSb, and InAs. The transmission peaks around 510 nm in the cell with the various thicknesses indicating the five materials. The transmission is due to the smaller bandgap of the active layer around 0.17 eV of its highest wavelength, 700nm. For InSb material, photon light absorbing for wavelength 350 [nm] works for ultraviolet light, which is not for photon light absorbing. This layer is working to collect a much higher transparency rate.

TABLE VI
 Comparison between different cells

Name of solar cell	Year	Open circuit voltage (V _{oc})	Fill factor (F.F.)	Efficiency (η%)
Perovskite cells [24]	2014	1.074	57.9	6.4%
TiO ₂ nanotube film [25]	2015	0.68	0.71	7.1%
Dye-sensitized solar cells[26]	2015	0.73	0.68	8.22%
Quantum Dotcells[27]	2020	0.58	0.52	13.49 %
Proposed Model	2023	0.61 V	0.6531	15.2655%

Several types of transparent cells have been developed, such as perovskite, dye sensitized, and Quantum Dot. However, the efficiency of many of these is still poor. Prior reports have revealed that dye sensitized performed low stability under UV-illumination [28] and insufficient control of the surface morphology of perovskite, causing low efficiency.

Due to high absorption and conductivity of AlGaAs,[29] and si exhibits high transparency and good conductivity [30] have been effectively utilized in our work inside; the effectiveness of transparent multi-coupled with low concentrator photovoltaic system was investigated. The results show that the system-coupled devices' overall performance is 15.2655% higher than other technology.

V. CONCLUSION

In summary, we have created transparent, near-infrared absorbing planar solar cells that are suitable for inclusion into architectural glass. These cells have a maximum power conversion efficiency of 15.2655% and an average visual transmission of 60%, which is sufficiently transparent to be used on structural glass. Here we examined the optical and electrical behaviour of cells. Our optical generation rate calculations, in particular the current-voltage characteristics, are presented. Due to the solid thermal conduction of layer thickness, the thermal trends of the cell have improved. The impact of temperature change and doping concentration on additional layers will be analyzed in further research. Finally, these devices serve as a roadmap for developing high-efficiency, high-transparency solar cells that could be used in glass to produce electricity, cut cooling costs, and recycle energy.

REFERENCES

- [1] B. Li, L. Wang, B. Kang, P. Wang and Y. Qiu, *Sol. Energy Mater. Sol. Cells*, 2006, 90, 549–573
- [2] Chau, J. L. H., Chen, R. T., Hwang, G. L., Tsai, P. Y., & Lin, C. C. (2010). Transparent solar cell window module. *Solar Energy Materials and Solar Cells*, 94(3), 588-591
- [3] Guha, Subhendu, Jeffrey Yang, and Baojie Yan. "High efficiency multi-junction thin film silicon cells incorporating nanocrystalline silicon." *Solar Energy Materials and Solar Cells* 119 (2013): 1-11
- [4] Abdelkader, M. R., Al-Salaymeh, A., Al-Hamamre, Z., & Sharaf, F. (2010). A comparative Analysis of the Performance of Monocrystalline and Multicrystalline PV Cells in Semi Arid Climate Conditions: the Case of Jordan. *Jordan Journal of Mechanical & Industrial Engineering*, 4(5)
- [5] Gall, S., Becker, C., Conrad, E., Dogan, P., Fenske, F., Gorka, B., ... & Rech, B. (2009). Polycrystalline silicon thin-film solar cells on glass. *Solar Energy Materials and Solar Cells*, 93(6-7), 1004-1008
- [6] Hegedus, S. (2006). Thin film solar modules: the low cost, high throughput and versatile alternative to Si wafers. *Progress in photovoltaics: research and applications*, 14(5), 393-411
- [7] Husain, A. A., Hasan, W. Z. W., Shafie, S., Hamidon, M. N., & Pandey, S. S. (2018). A review of transparent solar photovoltaic technologies. *Renewable and sustainable energy reviews*, 94, 779-791
- [8] Siddiki, Mahbube Khoda; Li, Jing; Galipeau, David; Qiao, Qiquan (2010). A review of polymer multijunction solar cells. , 3(7), 867–0
- [9] Torabi, N., Behjat, A., Zhou, Y., Docampo, P., Stoddard, R. J., Hillhouse, H. W., & Ameri, T. (2019). Progress and challenges in perovskite photovoltaics from single-to multi-junction cells. *Materials Today Energy*, 12, 70-94
- [10] Green, M. A., Emery, K., Hishikawa, Y., & Warta, W. (2010). Solar cell efficiency tables (version 37). *Progress in photovoltaics: research and applications*, 1(19), 84-92.
- [11] .Takamoto, T., Agui, T., Kamimura, K., & Kaneiwa, M. (2003, May). Multijunction solar cell technologies-high efficiency, radiation resistance, and concentrator applications. In 3rd World Conference on Photovoltaic Energy Conversion, 2003. Proceedings of (Vol. 1, pp. 581-586). IEEE.
- [12] Lin, H. W., Chen, Y. H., Huang, Z. Y., Chen, C. W., Lin, L. Y., Lin, F., & Wong, K. T. (2012). Highly efficient bifacial transparent organic solar cells with power conversion efficiency greater than 3% and transparency of 50%. *Organic Electronics*, 13(9), 1722-1728
- [13] Fu, F., Feurer, T., Jäger, T., Avancini, E., Bissig, B., Yoon, S., ... & Tiwari, A. N. (2015). Low-temperature-processed efficient semi-transparent planar perovskite solar cells for bifacial and tandem applications. *Nature communications*, 6(1), 8932
- [14] Ram, M. K., Sundaresan, N. S., & Malhotra, B. D. (1994). Performance of electrochromic cells of polyaniline in polymeric electrolytes. *Journal of materials science letters*, 13, 1490-1493.
- [15] Kim, G., Shin, M., & Lim, J. W. (2018, June). Investigation of transparent electrodes and transparent/opaque a-Si: H solar cells for indoor photovoltaics. In 2018 IEEE 7th World Conference on Photovoltaic Energy Conversion (WCPEC)(A Joint Conference of 45th IEEE PVSC, 28th PVSEC & 34th EU PVSEC) (pp. 338-340). IEEE.
- [16] Zandi, S., Saxena, P., Razaghi, M., & Gorji, N. E. (2020). Simulation of CZTSSe thin-film solar cells in COMSOL: Three-dimensional optical, electrical, and thermal models. *IEEE Journal of Photovoltaics*, 10(5), 1503-1507
- [17] Zandi, Soma; Saxena, Prateek; Gorji, Nima E. (2020). *Numerical simulation of heat distribution in RGO-contacted perovskite solar cells using COMSOL. Solar Energy*, 197(0), 105–110
- [18] J. Clerk Maxwell, *A Treatise on Electricity and Magnetism*, 3rd ed., vol. 2. Oxford: Clarendon, 1892, pp.68–73
- [19] Palik, E. D. (Ed.). (1998). *Handbook of optical constants of solids* (Vol. 3). Academic press.
- [20] Adachi, S. (2013). *Optical constants of crystalline and amorphous semiconductors: numerical data and graphical information*. Springer Science & Business Media
- [21] O.J. GLEMBOCKI, KENICHI TAKARABE, in *Handbook of Optical Constants of Solids*, Volume 2, 1998
- [22] Palik, E. D. (Ed.). (1998). *Handbook of optical constants of solids* (Vol. 3). Academic press.() Aspnes, D. E., & Studna, A. A. (1983). Dielectric functions and optical parameters of si, ge, gap, gaas, gasb, inp, inas, and insb from 1.5 to 6.0 ev. *Physical review B*, 27(2), 985
- [23] Energy bandgap of AlGaAs", *Batop.de*, 2022. [Online]. Available:https://www.batop.de/information/EgAlGaAs.htmlAccessed: 08- Aug- 2022]
- [24] Jung, H. S., & Park, N. G. (2015). Perovskite solar cells: from materials to devices. *small*, 11(1), 10-25.
- [25] Yang, D., Zhang, X., Hou, Y., Wang, K., Ye, T., Yoon, J., ... & Priya, S. (2021). 28.3%-efficiency perovskite/silicon tandem solar cell by optimal transparent electrode for high efficient semitransparent top cell. *Nano Energy*, 84, 105934
- [26] Han, L., Fukui, A., Chiba, Y., Islam, A., Komiya, R., Fuke, N., ... & Shimizu, M. (2009). Integrated dye-sensitized solar cell module with conversion efficiency of 8.2%. *Applied Physics Letters*, 94(1).
- [27] Rao, H., Zhou, M., Pan, Z., & Zhong, X. (2020). Quantum dot materials engineering boosting the quantum dot sensitized solar cell efficiency over 13%. *Journal of Materials Chemistry A*, 8(20), 10233-10241.
- [28] Qureshi, M., Chetia, T. R., Ansari, M. S., & Soni, S. S. (2015). Enhanced photovoltaic performance of meso-porous SnO 2 based solar cells utilizing 2D MgO nanosheets sensitized by a metal-free carbazole derivative. *Journal of Materials Chemistry A*, 3(8), 4291-4300.
- [29] Hussain, I., Tran, H. P., Jaksik, J., Moore, J., Islam, N., & Uddin, M. J. (2018). Functional materials, device architecture, and flexibility of perovskite solar cell. *Emergent Materials*, 1(3), 133-154
- [30] Vohl, P., Perkins, D. M., Ellis, S. G., Addiss, R. R., Hui, W., & Noel, G. (1967). GaAs thin-film solar cells. *IEEE Transactions on Electron Devices*, 14(1), 26-30



Maria Sultana Rupa holds the distinction of being the first female Inspection Audit Engineer at Creative Engineers Ltd, an esteemed company merging with Schindler in the Elevator Industry of Bangladesh. She completed her BSc and MSc at the Department of Electrical and Electronic Engineering, Faculty of Engineering, American

International University - Bangladesh, from January 2017 to December 2020. Subsequently, she pursued her MSc from 2021 to 2023, graduating with an MSc. (EEE) degree, marked by the prestigious "Dean's List Honor" academic distinction in 2023.

Throughout her academic journey, Maria secured a noteworthy general waiver of 25% from January 2021 to December 2023. Her dedication to academic excellence was further acknowledged as she earned the esteemed "Magna Cum Laude" academic distinction from American International University- Bangladesh, Dhaka, Bangladesh, for her exceptional performance during her MSc program. In her undergraduate project and thesis, Maria collaborated on the "DESIGN AND IMPLEMENTATION OF SOLAR, WIND, AND PIEZOELECTRIC HYBRID POWER SYSTEM." This innovative project aimed to deliver efficient power solutions to clients while prioritizing environmental sustainability. Each power source featured its intricate circuit comprising inverters and transformers, converging to form an integrated hybrid power system. Maria actively engaged in enriching her knowledge through participation in various webinars hosted by the University of Rajshahi and American International University – Bangladesh. Her involvement extended to esteemed organizations such as Udemy, COURSERA, Comsol Multiphysics, NANO HUB, and nanotechnology@aiub. Her research pursuits and interests span a diverse spectrum including nanostructures, nanotechnology, microelectronics, nanoelectronics, nanomaterials, photovoltaics, Piezoelectric sensors, IoT, solar cells, mid-infrared emitters and receivers, VLSI, Analog and Mixed Circuit and IC design, medical devices, sensors, and biosensors.



Dr. M. Tanseer Ali has completed his B.Sc. in Electrical and Telecom Engineering from North South University, Dhaka in 2007. Then he pursued higher studies and received M.Sc. in Communication Engineering with Distinction from Robert Gordon University, Aberdeen, UK, in 2008. He received a full scholarship from the

University of Greenwich, London, UK, for the Ph.D. degree. He completed his doctorate in 2013. Currently, he is working as a Senior Assistant Professor at the Department of EEE, Faculty of Engineering, AIUB, Dhaka. His research interest is in Microwave Circuit and Systems, Antenna Design, Nanoelectronics, CMOS Circuits, VLSI, Analog and Mixed Circuit and IC Design, Quantum Properties of materials, Engineering Education, and Pedagogy.



Mohammad Abdul Mannan received his B. Sc. Eng. Degree from Rajshahi University of Engineering and Technology (RUET former BITR), Bangladesh, in 1998, and Masters of Eng. and Dr. of Eng. degrees from Kitami Institute of Technology, Japan, in 2003 and 2006 respectively, all in electrical engineering.

He then joined in the American International University Bangladesh (AIUB) as an Assistant professor in May 2006. He served in AIUB as an Associate Professor from December 2013 to November 2016. Now he is working as a Professor and Director of Faculty of Engineering in AIUB. His research interests include electric motor drive, power electronics, power system, wind generation system and control of electric motor, power electronic converters, power system, and wind generation system. Prof. Dr. Mannan is a member of the IEB and IEEE.



Mr. Mehedi Hasan is an Assistant Professor at the Dept. of EEE, since 2018, Faculty of Engineering, American International University- Bangladesh (AIUB). He accomplished his B.Sc. Engg. (EEE) and M.Sc. Engg. (EEE) degree with the 'Summa Cum Laude' academic distinction from American International University-

Bangladesh, Dhaka, Bangladesh in 2012 and 2014 respectively. Mehedi Hasan started his teaching career as a Teaching Assistant in Dept. of EEE and served from September 1, 2013, to January 13, 2015. Previously, he worked as a Lecturer for the duration of 3+ years at AIUB in his own department. As a researcher, he has published several research articles in various internationally renowned journals. He elected as a judge in different Math Olympiad, Math Quiz Contest, AIUB Jubilation, Science Congress seminars, Robotics Contest and Programming Contest. He participated various symposium, international conferences, seminars, workshops, and industrial tours in different places. He is also a Professional of IEEE USA, Member of the OBE Committee in AIUB and Committee Member of iCREST. His research interests Nanotechnology, Characterization of nano particles, Quantum Mechanics, Nanoparticle, Nano transistor, Spintronics, nano- photonics, Nano sensor, Band Structure Model, Material synthesis and characterization, green synthesis, PCF, SPR, Biosensor, solar cell, piezoelectric sensor, IoT, Deep learning(AI), VLSI & ULSI Design, Quantum wire, Quantum Dot related works.